




Article

Optimization Study of Cooling Channel for the Oil Cooling Air Gap Armature in a High-Temperature Superconducting Motor

Shuai Yu ^{1,2}, Yong Zhou ^{3,*} , Yongmao Wang ^{1,2,*}, Ji Zhang ⁴, Qi Dong ³, Jie Tian ^{1,2}, Jing Chen ^{1,2} 
and Feng Leng ^{1,2} 

¹ Hubei Key Laboratory of Marine Electromagnetic Detection and Control, Wuhan 430205, China; yus.2012@tsinghua.org.cn (S.Y.); tianjie_2006@hust.edu.cn (J.T.); drchen@whu.edu.cn (J.C.); lengfeng@hust.edu.cn (F.L.)

² Wuhan Second Ship Design and Research Institute, Wuhan 430205, China

³ Wuhan Institute of Marine Electric Propulsion, Wuhan 430064, China; xlfu@tongji.edu.cn

⁴ College of Electrical and Information Engineering, Hunan University, Changsha 410082, China; jizhang@hnu.edu.cn

* Correspondence: zhouy18@lzu.edu.cn (Y.Z.); m201071098@hust.edu.cn (Y.W.)

Abstract: With the continuous advancement of science and technology, the application of high-temperature superconductivity has developed rapidly. The high-temperature superconducting (HTS) motor replacing the copper coil in the traditional motor with HTS winding is increasingly used in power equipment, and the effective thermal management of HTS winding is vital in ensuring the life and effective operation of the HTS motor. In this study, five enhancement structures of indirect oil cooling channels were designed to improve the heat dissipation capacity of the HTS motor winding, and the enhancement effects of the different structures were comprehensively evaluated through numerical simulation using Fluent software 2022R1. The best enhancement structure was selected through structural optimization. The results showed that the Nusselt number of the gap-type enhanced structure was higher than that of the V- and staggered-type structures at the same flow velocity and 68% higher than that of the bare pipe. At the same inlet flow velocity and with a pressure drop limit of 30 kPa, the performance evaluation criterion value of the gap-type structure was 39% and 63% higher than that of the staggered- and V-type structures, respectively. The gap type is the optimal enhancement structure and can effectively improve the heat dissipation of the HTS winding coil.

Keywords: high-temperature superconducting motor cooling; indirect oil cooling; numerical simulation; heat transfer enhancement



Citation: Yu, S.; Zhou, Y.; Wang, Y.; Zhang, J.; Dong, Q.; Tian, J.; Chen, J.; Leng, F. Optimization Study of Cooling Channel for the Oil Cooling Air Gap Armature in a High-Temperature Superconducting Motor. *Electronics* **2024**, *13*, 97. <https://doi.org/10.3390/electronics13010097>

Academic Editor: François Auger

Received: 17 October 2023

Revised: 14 December 2023

Accepted: 20 December 2023

Published: 25 December 2023



Copyright: © 2023 by the authors. Licensee MDPI, Basel, Switzerland. This article is an open access article distributed under the terms and conditions of the Creative Commons Attribution (CC BY) license (<https://creativecommons.org/licenses/by/4.0/>).

1. Introduction

With the advancement of science and technology, the propulsion system of power equipment continues to shift to electrification. The motor is the core component of the electric propulsion system, but the traditional motor is larger, and the power density is relatively low. High-temperature superconducting (HTS) motors [1] combine superconducting technology and motor technology, replacing the copper coil in the traditional motor with an HTS coil and then combining them with low-temperature refrigeration systems to ensure their superconducting state. Compared with the same power and the same speed of the traditional motor, the HTS motor has the advantages of miniaturization, low weight, high power density, etc., and has broad application prospects in the fields of marine electric propulsion [2,3], direct-drive (DD) wind power generation [4,5], and electric aircraft propulsion [6] with strict requirements for power density and bulk density. Since an HTS wire of the same size as a copper wire can carry a current about 100 times higher than that of the copper wire, the excitation coil wound from it can generate a high magnetic field of more than 2 t in the motor, which is the magnetic saturation point of the core material.

Therefore, the stator of the HTS motor generally uses non-magnetic materials, such as glass fiber-reinforced plastic (GFRP), to replace the air gap armature structure of the iron teeth to eliminate the serious magnetic saturation and several times the core loss caused by the air gap magnetic density in the stator core tooth, but compared with the iron core stator, the thermal conductivity of the air core stator is lower, and the heat of the stator coil cannot be effectively conducted out; moreover, the coil is directly placed in the air gap of the HTS motor, and most of the tangential electromagnetic force of the air core stator directly acts on the coil. In addition, due to the large magnetic flux of the HTS magnet through the winding, the eddy current loss of the air gap winding is larger than that of the traditional stator coil [5]. This leads to an increase in the temperature of the air gap armature, and the temperature rise of the air gap armature affects the performance and life of the motor. As electric motors are developed to achieve high power density, miniaturization, and low weight [7,8], the internal heat generation of these motors increases dramatically, and the effective heat dissipation space is relatively limited. As a result, the performance and life of the motors are affected. Determining how to implement effective thermal management of electric motors and inhibit the temperature rise of air gap armature is crucial to ensuring the efficient and stable operation of motors.

At present, air, liquid, and evaporative cooling are often used to achieve motor cooling. Evaporative cooling utilizes the vapor–liquid phase change cycle of the working fluid to achieve efficient motor cooling. It is suitable for megawatt-class, large-capacity power generation systems, but its system complexity and maintenance difficulties limit its application in kilowatt-class motor heat dissipation [9]. Air cooling heat dissipation systems often rely on free convection [10] for the outer part of the motor and forced convection [11,12] for the inner part to achieve heat dissipation. Air cooling heat dissipation systems are simple, reliable, and inexpensive, but the low thermal conductivity of air results in poor heat dissipation efficiency; these systems are suitable for motors with low to medium heat flow density or large motors with a sufficient heat transfer area [13]. Compared with air cooling, liquid cooling has better cooling efficiency and is noiseless. It is widely used in high-power-density motors. Depending on the cooling medium, liquid cooling systems can be mainly divided into two categories: water and oil cooling systems. Water is often used as a cooling medium because it is easy to obtain and has low viscosity, high heat capacity, and high thermal conductivity. The heat generated by the motor is removed by the circulating flow of water in the internal cooling channel of the housing, but the air gap has high thermal resistance in this cooling method. To overcome this shortcoming, scholars have introduced a compact cooling method in which several water-cooling plates with a large heat transfer area are radially inserted into the core laminations to increase the heat transfer effect [14]. However, water-cooling conduit connections are complicated, and most of them are suitable only for stator cooling; they cannot directly cool the motor winding, a part that cannot easily dissipate heat. Moreover, water has a high freezing point and a low boiling point. The process of long-term cycling causes scale corrosion of the housing, which entails risks of clogging and leakage, thereby threatening the safety of the motor [15]. For the cooling of the air gap armature in the case of high stator heat load, conventional cooling, such as air cooling, can not meet the heat dissipation requirements of the air gap armature, and water cooling has certain safety risks. At present, the more suitable cooling method is liquid cooling, which mainly includes winding liquid internal cooling [16], channel liquid cooling [17], and oil cooling [18,19] as the three cooling methods. Compared with the previous two cooling methods, oil has advantages, such as excellent insulation characteristics, high reliability, a high dielectric constant, a low freezing point, and a high boiling point, which can improve the adaptability of the motor system to the external environment and prevent corrosion hazards, such as cavitation and scaling. Therefore, an oil cooling scheme was adopted to improve the heat dissipation effect of the air gap armature stator of the high-temperature superconducting motor.

Oil cooling is divided into direct and indirect oil cooling. Oil has excellent insulation characteristics, so it can directly immerse key heating components, such as the stator and

winding inside the motor, in cooling oil [20] or make the cooling oil come into direct contact with the inner surface of the housing or the end of the stator through spraying [21,22], thereby removing the heat of the motor. The cooling efficiency of direct oil cooling is higher than that of water cooling and indirect oil cooling. However, due to the high viscosity of the oil medium, direct oil cooling increases the resistance of the rotor during rotation. When the motor stops working, if the oil is exposed to a low-temperature environment for a long time, it may condense when the motor restarts and cause serious power loss. Spread oil cooling works only on the end windings; the contact area with the windings is too small, and the heat transfer capability is weak [23]. In addition, the impurities in the oil medium can damage the insulation inside the motor, thus increasing the risk of damage to the motor.

Indirect oil cooling avoids direct contact with the internal parts of the motor and is more controllable. Indirect oil cooling is similar to water cooling in that it also removes heat by circulating the cooling oil through the flow channels [24]. The windings in the motor are the main heat source, and the direct contact between the windings and the oil-based cooling channels not only reduces the thermal resistance of the gap between the cooling water channels in the housing and the windings when water is used as the medium but also makes the process more controllable than direct oil cooling. However, unlike indirect oil cooling, the inclusion of cooling channels affects the heat dissipation effect of the windings. Other ways to improve the cooling efficiency of indirect oil cooling must be explored to ensure the reliability of cooling while compensating for the poor cooling efficiency. Figure 1 shows several cooling methods commonly used at present [25].

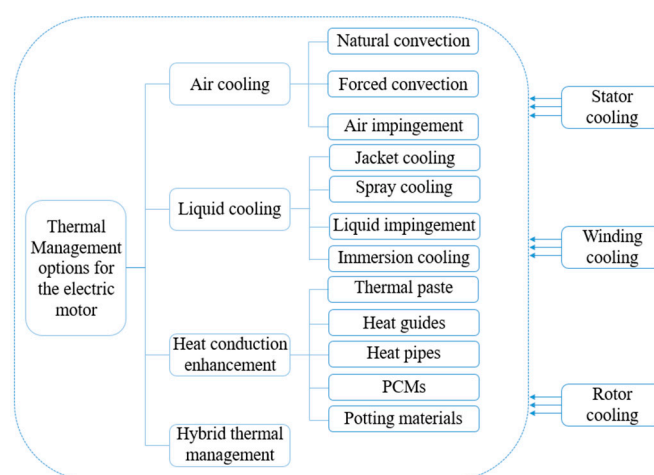


Figure 1. Common motor cooling methods.

To improve the cooling efficiency of indirect oil cooling, researchers have used end-face oil covers and cooling oil channels inside the stator to simultaneously cool the stator and end windings and improve the cooling effect [26]. In recent years, researchers have also used slot cooling technology, which is different from direct and indirect oil cooling; they optimized the geometry and location of the slots through simulation, and on the basis of the optimization results, prototypes were built and tested to investigate the effect of slot geometry on the cooling effect of the motor [27]. The research on the water-cooled cooling channel structure is relatively mature. A fin structure is added to the inner surface of the cooling water jacket, which is placed between the windings, and the heat generated by the windings is directly conducted by the fins to the U-type water pipe inside the fins and subsequently removed by the coolant inside the water pipe [28]. A group of scholars selected an optimal cooling channel by comparing and analyzing the cooling effect of the cooling channel with those of the spoiler, spiral structure, tandem structure, and Z-shaped structure inside the channel; then, the optimal parameter for improving the cooling efficiency was obtained by optimizing the number of channels and radial and axial

lengths of the cooling structure [29]. Most of the abovementioned cooling methods are used for the optimization of the water-cooling channel structure, but large differences exist between the properties of water and oil and between slot and indirect oil cooling. Only a few studies have attempted to change the channel structure of indirect oil cooling to improve the cooling efficiency of the motor. Thus, the effects of different channel structures on the heat exchange effect of indirect oil cooling need to be studied.

In this study, to strengthen the cooling efficiency of indirect oil cooling channels, the influence of five enhanced structures inside a stainless steel pipe on the heat dissipation of the coil was investigated through Fluent numerical simulation. The average temperature of the outlet surface of the stainless steel pipe was used as the evaluation index and compared with the average temperature of the bare pipe to determine the enhancement result of the different structures. Three enhancement structures with strong performance were identified. Furthermore, the pressure drop, heat transfer coefficient, Nusselt number, friction factor f , and performance evaluation criterion (PEC) of the three superior enhancement structures were calculated at different flow rates under the condition of limited pressure drop to comprehensively evaluate the cooling effects of the structures, ultimately determining the optimal enhancement structure.

2. Methods

2.1. Geometries of the Oil Cooling Channel

The cooling system structure is shown in Figure 2. The flow channel was close to both sides of the stator teeth and was in direct contact with the centralized winding, the cooling medium flowed through the flow channel in the stator groove along the axial direction, and the stator winding and the core were cooled at the same time.

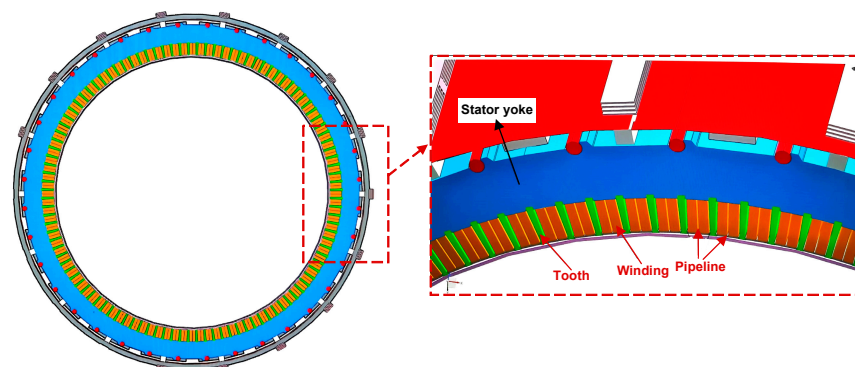


Figure 2. Schematic diagram of the cooling channel of the motor.

Figure 3a shows the physical model of the oil cooling. The stainless-steel pipe (oil cooling channel) was located in the middle of the two winding coils. Figure 3b shows the dimensions of the stainless-steel pipe. The cooling channel's length, height, and width were 700, 36.4, and 1.5 mm, respectively, and the thickness of the stainless-steel tube was 0.8 mm. Table 1 presents the five types of enhancement structures.

Table 1. Different channel structures.

Channel Structure	Enhancement Pattern
Structure 1	/
Structure 2	Staggered type
Structure 3	Gap type
Structure 4	V type
Structure 5	Cylindrical type
Structure 6	Parallel type

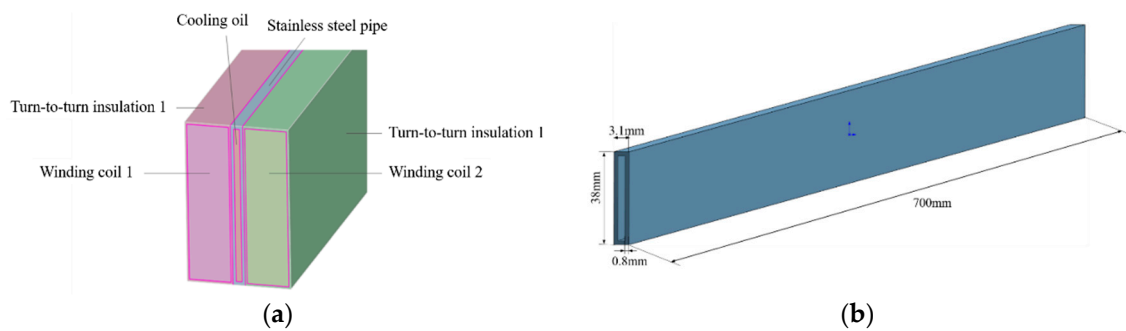


Figure 3. (a) Oil cooling physical model and (b) the stainless-steel pipe's size.

Diagrams of the different enhancement structures are illustrated in Figure 4. Structure 1 was a bare pipe, and no enhancement structure was present inside the pipe. Structure 2 was a staggered flat plate (Figure 4a). The flat plate structure could increase the disturbance effect on the oil, thus increasing the retention time of the cooling oil in the stainless-steel pipe and enhancing the heat transfer. The two adjacent flat plates could also change the direction and speed of the oil flow. Structure 3 was a gap-type plate structure (Figure 4b) that was adjacent to the two flat plates. It could increase the disturbance of the oil flow, and the disturbance was aggregated and then diverted, resulting in a great oil flow disturbance effect compared with Structure 2. Structure 4 was a V-type flat plate (Figure 4c). The angle between two flat plates was 30° to extend the retention time of the fluid in the pipe, produce reflux, and obtain an improved heat transfer effect. Structure 5 was a cylindrical plate (Figure 4d) that used multiple sets of cylinders for the fluid shunt effect. Through continuous dispersion, the velocity and direction of the fluid were changed to enhance the heat transfer. Structure 6 was a parallel-type flat plate (Figure 4e). Numerous parallel-type flat plates were employed for the fluid shunt, and the coil part of the heat first transferred to the flat plates was taken away by the oil.

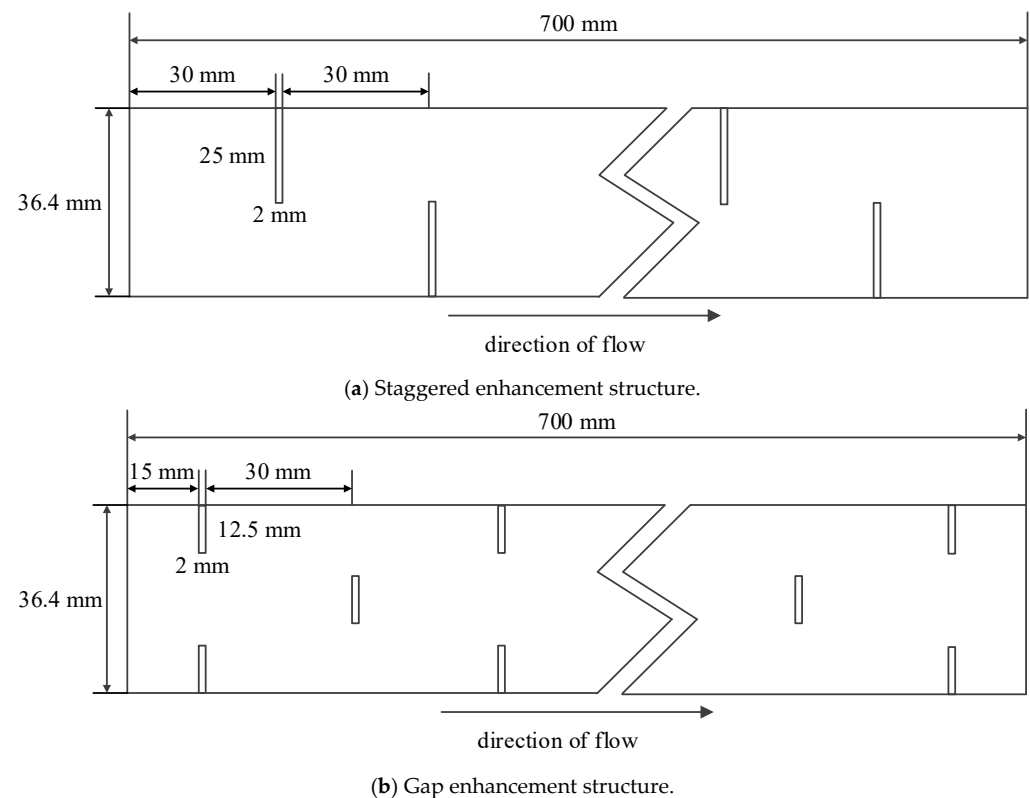


Figure 4. Cont.

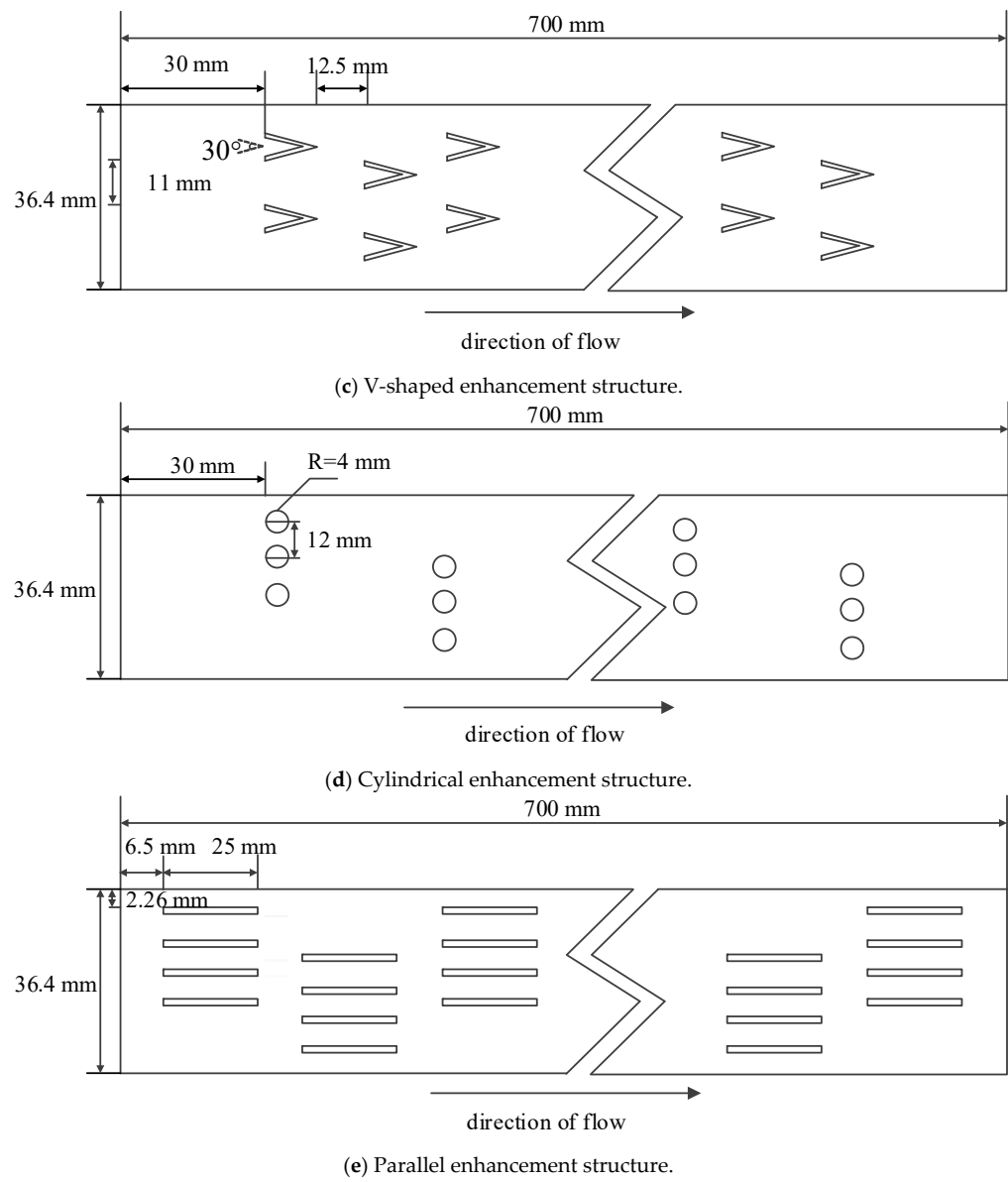


Figure 4. Different enhancement structures.

2.2. Evaluation Indicators

According to the numerical simulation results, the pressure drop, heat transfer coefficient h , Nusselt number, friction factor f , and PEC values were calculated for a comprehensive comparison of the performance among the six oil-cooling channels. Table 2 shows the inlet velocities of the oil flow used in the numerical study, accompanied by the Reynolds number.

(1) The Nusselt number is calculated by:

$$Nu = \frac{hD_h}{\lambda}, \quad (1)$$

where λ is the thermal conductivity of the oil and D_h is the hydraulic diameter of the cooling channel, calculated by:

$$D_h = \frac{4A_c}{P}, \quad (2)$$

where Ac is the cross-sectional area of the pipe, P is the wetted perimeter, and h is the convective heat transfer coefficient, defined as:

$$h = \frac{q_w}{\Delta T}, \quad (3)$$

where q_w is the heat flux of the heated wall surface and ΔT is the difference between the average temperature of the wall surface (area average) and the average temperature of the fluid.

- (2) Friction factor f is computed as:

$$f = \frac{\Delta P}{\frac{1}{2}\rho\mu^2} \cdot \frac{D_h}{l}, \quad (4)$$

where ΔP is the pressure difference between the inlet and outlet, μ is the inlet velocity, ρ is the fluid density, and l is the pipe length.

- (3) The performance evaluation criterion (PEC) is calculated as:

$$PEC = \frac{\frac{Nu}{Nu_0}}{(f/f_0)^{\frac{1}{3}}}, \quad (5)$$

where Nu and f are the Nusselt number and friction factor of the enhancement structure channel, respectively, and Nu_0 and f_0 are the Nusselt number and friction factor of the bare pipe, respectively.

Table 2. Correspondence between inlet velocity V and Reynolds number Re .

μ (m/s)	0.087	0.13	0.173	0.217	0.26	0.3	0.4	0.5
Re	25	37.5	50	62.5	75	86.4	115.2	144

2.3. Model Validation

In this section, we model a cooling channel that has a similar flat structure to the target stainless-steel pipe in the present study (see Figure 3b) and was experimentally tested in Ref. [30]. Furthermore, we validate the numerical model on the basis of the test data obtained in Ref. [30].

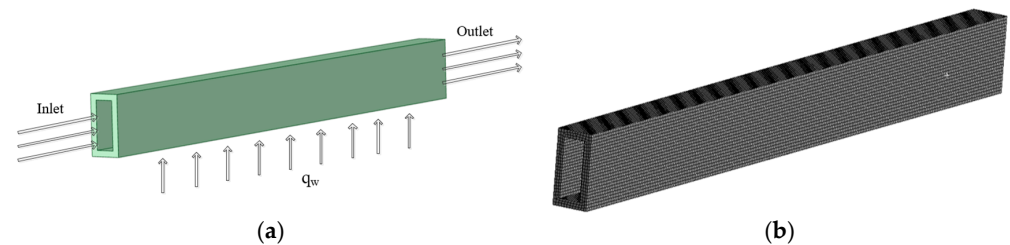
The model parameters in the cooling channel are shown in Table 3, where L , W , H , and σ are the length, width, height, and pipe thickness of the cooling channel, respectively. The material physical parameters are shown in Table 4. The pipe wall material was silicon, and water was selected as the working fluid. The established physical model (Figure 5a) and meshing (Figure 5b) are shown in Figure 5. All the simulations were performed with Ansys Fluent, and the calculations used the simple algorithm. The validation model was assumed to have a smooth inner wall; only the bottom had a constant heat flux, and all other walls were adiabatic. The value of the heat flux at the bottom was 100 W/cm^2 , the inlet velocity was 0.19 m/s , the inlet temperature was 26.85°C , and it was a pressure outlet. The number of divided grid cells was 625,000.

Table 3. Model parameters.

Parameter	Value (mm)
L	10
W	0.3
H	0.9
σ	0.1

Table 4. Parameters of material properties.

Material	ρ (kg m^{-3})	c_p ($\text{J kg}^{-1} \text{K}^{-1}$)	k ($\text{W m}^{-1} \text{K}^{-1}$)	u ($\text{kg m}^{-1} \text{s}^{-1}$)
Fluid (water)	998.2	4182	0.6	0.001003
Solid (Si)	2328.3	700	148	--

**Figure 5.** (a) Verification model and (b) mesh.

When the Reynolds number was 100, the flow inlet velocity obtained through calculation was 0.19 m/s, and the temperature distribution at the bottom surface of the pipe along the centerline direction was simulated for comparison with known literature results. Figure 6 shows the bottom surface temperature distributions in the simulation. The temperature distribution of the original rectangular smooth channel in this study was simulated and verified (Ref. [30]), and the temperature distribution on the bottom surface of the pipe in Case 0 was compared. Both exhibited the stratification phenomenon, and the temperature distribution trend was consistent, which indicates that the model established in this study has high accuracy.

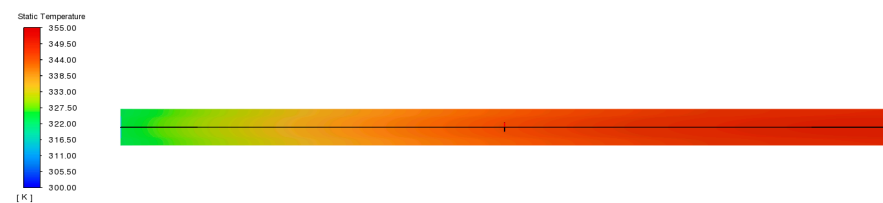
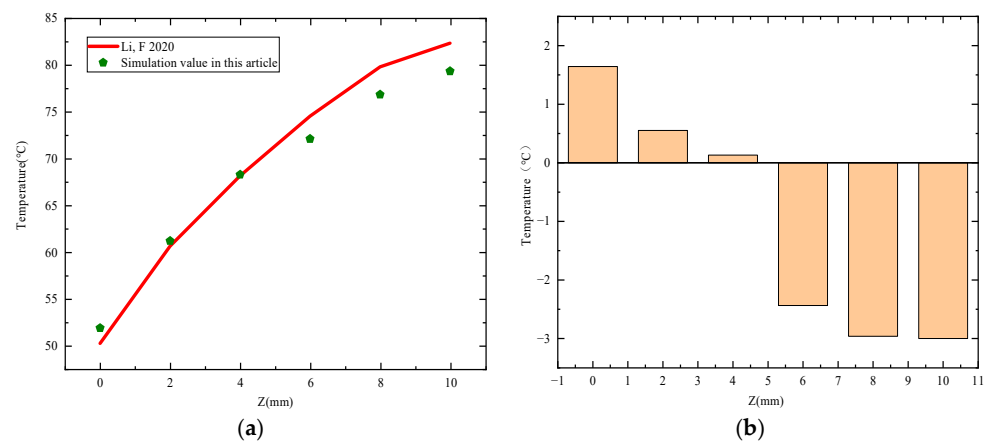
**Figure 6.** Temperature distribution on the bottom surface of the pipe.

Figure 7 shows the pipe length in the 0–5 mm interval. The simulation and existing literature values agreed, as indicated in the figure. The two errors were relatively small. The 5–10 mm interval was slightly different. The simulated temperature gap was the largest at 10 mm, the maximum temperature difference was only about 3 °C, and its maximum error was about 1.603%. These results show that the model used in this study has high accuracy.

**Figure 7.** Data validation: (a) comparison of temperature changes between simulated and reference data [30] and (b) temperature difference between simulated and reference values.

3. Screening of Five Enhancement Structures

3.1. Velocity and Temperature Distributions of Different Enhancement Structures

Numerical simulations were conducted for the six flow channel structures mentioned in Section 2.1 under the following operating conditions: inlet oil velocity of 0.19 m/s, inlet temperature of 40 °C, and coil heat generation of 380,000 W/m³. The overall number of grid units for the nonreinforced structures was 817,830. The number of grid units for the enhancement structures was controlled between 6 and 8 million and stabilized within 600 s. This section focuses on the effects of the different enhancement structures inside the pipe on coil heat dissipation, and the average temperature of the outlet surface was used as an evaluation indicator.

Figure 8 presents a temperature distribution cloud map of the six cooling channels. The temperature of the bare pipe (Figure 8a) increased uniformly in the direction of fluid flow and was affected by wall heat transfer, resulting in a high temperature near the wall. With the enhancement structures, the fluid temperature changes inside the different structures varied. Specifically, the staggered enhancement structure (Figure 8b) showed a continuous increase in temperature along a specific trajectory. In the gap-type enhancement structure (Figure 8c), in which the fluid first gathers and then disperses, the fluid temperature in the area near the inlet side was higher than that in the other areas. The V-type enhancement structure (Figure 8d) had a much higher temperature in the angle region than in the other regions, mainly because of fluid stagnation in this region. The cylindrical enhancement structure (Figure 8e) had almost no stagnant area and exhibited good fluid flow performance. The parallel enhancement structure (Figure 8f) showed little change in fluid temperature. Only the flat structure had a considerable increase in heat conduction temperature, but the area where the fluid flushed the flat plate was small, resulting in the inability to effectively remove heat.

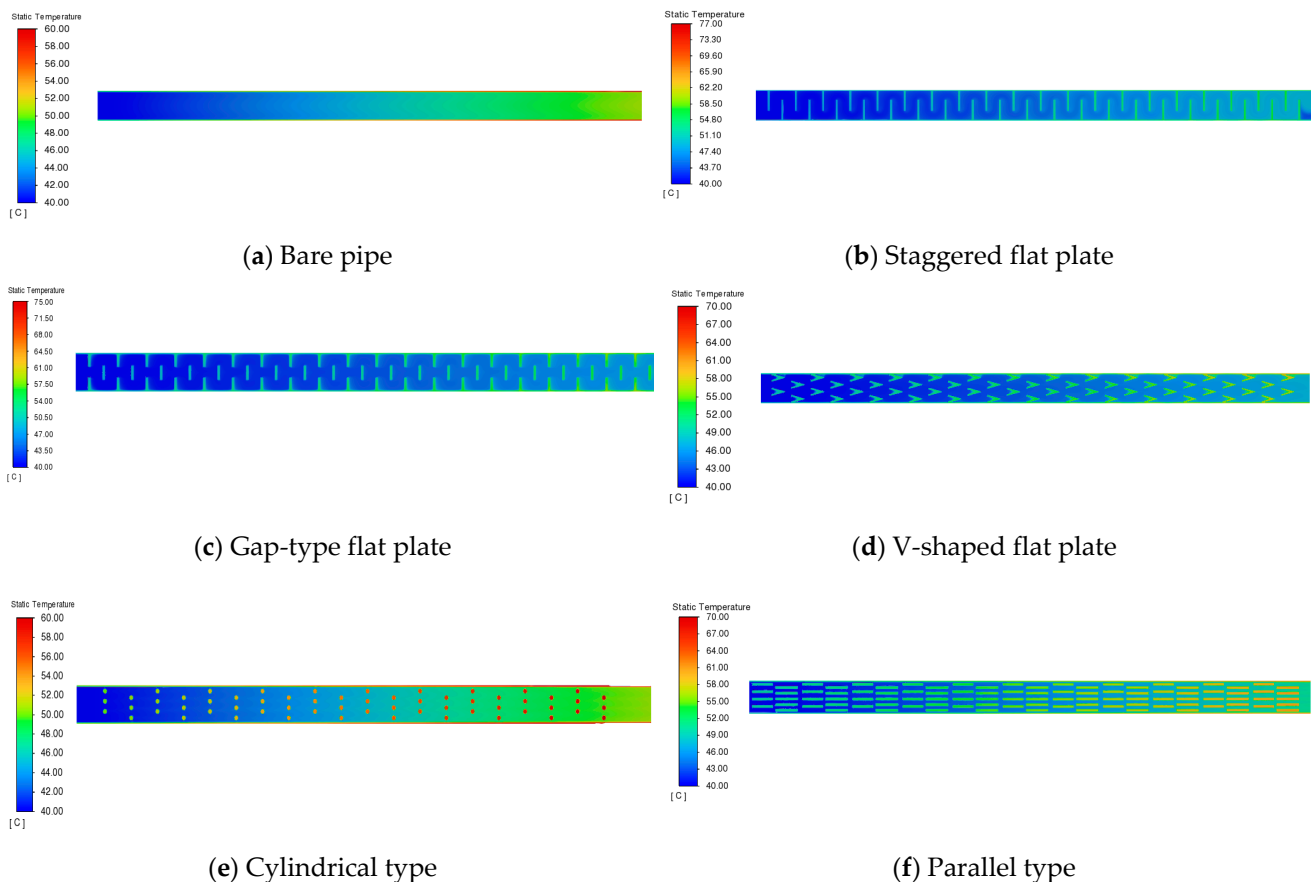


Figure 8. Temperature distribution of different enhancement structures.

Figure 9 shows the flow velocity distribution cloud map of the fluid at 600 s. The flow velocity inside the bare pipe (Figure 9a) was stable at 0.19 m/s, whereas the fluid in the enhancement structure exhibited the reflux phenomenon. The staggered enhancement structure (Figure 9b) followed the fluid trajectory, and the velocity in each region of the trajectory was the same. The velocity reached its maximum at the end of the flat plate, and the velocity near the wall was almost zero. The gap-type enhancement structure (Figure 9c) was similar to the V-type strengthening structure (Figure 9d); the highest flow velocity was between the plates in the radial cross-section. The gap-type structure, in which the velocity of the flow near the wall tends to be zero, presented considerably limited heat transfer performance, whereas the staggered flat plate performed well and had a relatively small stagnation zone. The cylindrical enhancement structure (Figure 9e), in which the cylinder causes fluid flow separation, had the highest velocity at the confluence point passing over the cylinder. The parallel enhancement structure (Figure 9f) was similar to the cylindrical structure in that the velocity reached its maximum between the parallel plates and remained at its maximum along the length of the plates.

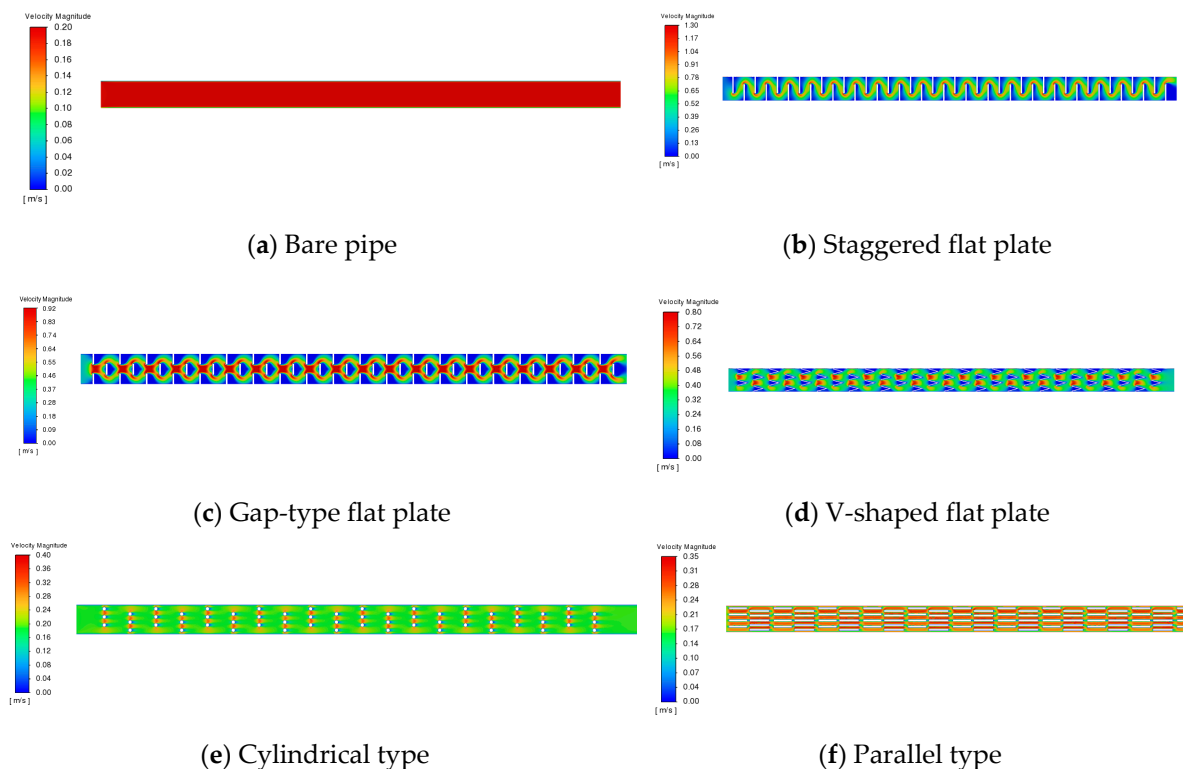


Figure 9. Elocity distribution of different enhancement structures.

Figure 10a shows the average temperatures of the outlet surfaces of the channels with different enhancement structures. The average temperature of the staggered structure was 51.59 °C, which was 2.73 °C higher than the average temperature of the bare pipe structure (i.e., 48.85 °C). From the perspective of the heat transfer temperature difference, the enhancement effect was about 30.84%, which indicated that the staggered structure had the best performance among all the enhancement structures. The average temperature of the V-type structure was 49.58 °C, which was 0.73 °C higher than that of the bare pipe and slightly higher than that of the gap structure (49.31 °C) and cylindrical structure (49.29 °C). The parallel structure had the worst average temperature of the five enhancement structures. Its average temperature was only 0.23 °C higher than that of the bare pipe. Figure 10b illustrates the average fluid temperatures. The V-type structure fluid had the highest average temperature mainly because this structure had the largest stagnation region in the enhanced heat transfer process. Figure 10c shows the maximum temperature of the fluid. The maximum temperature

of the fluid in the staggered and cylindrical structures was close to 61 °C, which was much higher than the maximum temperature of 50.37 °C in the case of the bare pipe.

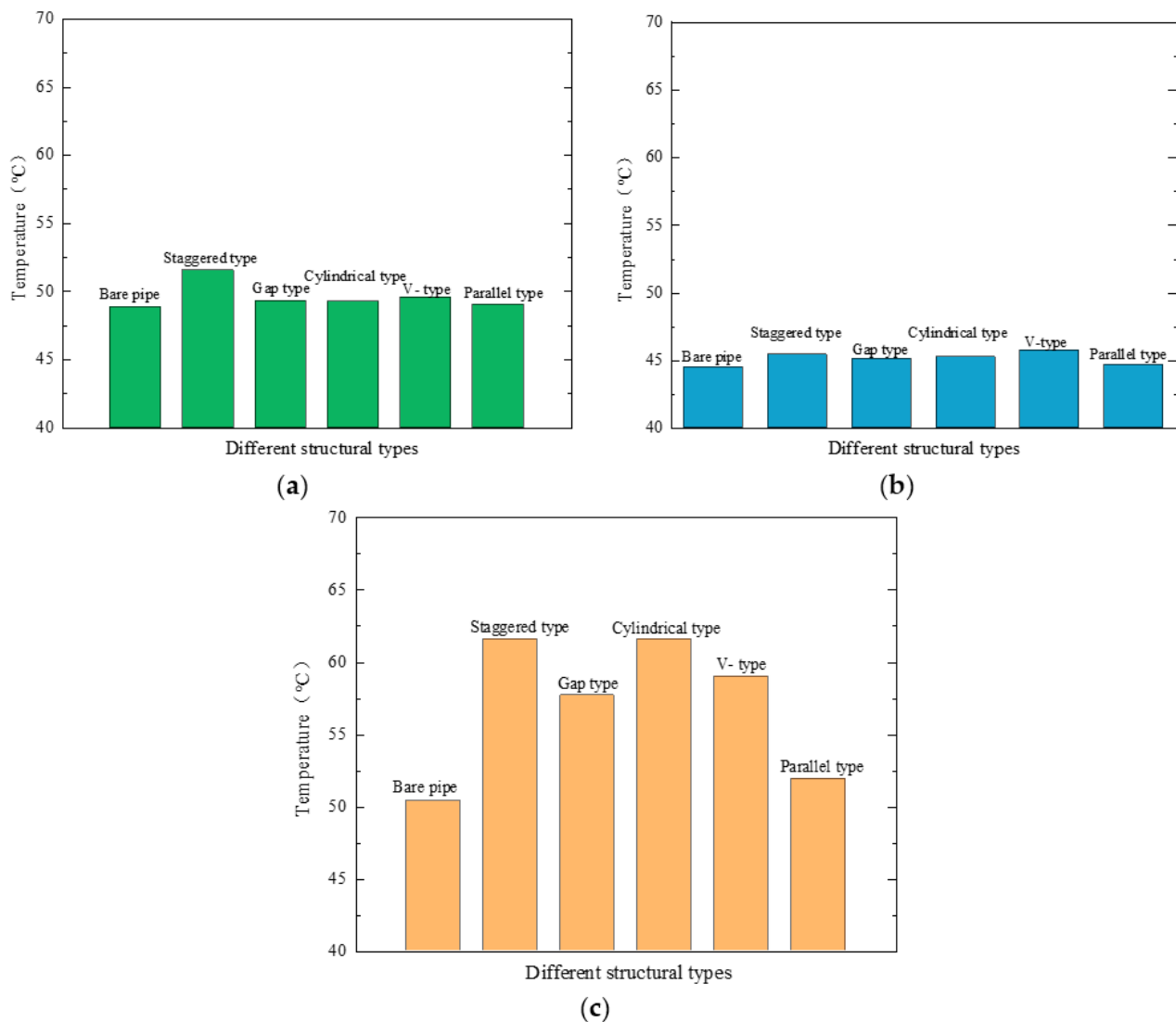


Figure 10. Variation in the (a) average temperature of outlet surface, (b) average fluid temperature, and (c) maximum fluid temperature with different structural types.

Figure 11a shows the average flow velocity. The staggered-type structure had the highest average flow velocity. According to Figure 11b, the maximum flow velocity of the staggered-type structure was the highest, and although the maximum flow velocities of the V- and gap-type structures also exceeded 1 m/s, they were limited to a very small area, and the average flow velocity was slightly higher than the initial velocity. The parallel type was similar to the cylindrical type. Its average flow velocity was slightly higher than that of the cylindrical type due to the maximum velocity between the flat plates and because the area of maximum velocity was larger than that of the cylindrical type.

3.2. Effects of Reynolds Number on the Performance of Different Enhancement Structures

Figure 12 displays the change in pressure drop with the Reynolds number for the different enhancement structures. The disturbing element increased the pressure drop. The pressure difference between the inlet and outlet of the pipe under the same inlet flow rate was enlarged, and the pressure drop of the different enhancement structures increased with the increase in the Reynolds number. The effects of the different structures on the pressure drop were not obvious when the Reynolds number was low, but the pressure drop varied

greatly at high Reynolds numbers. The pressure drop of the bare pipe varied the least, followed by that of the gap type. Meanwhile, the increase in the staggered-type structure was particularly obvious.

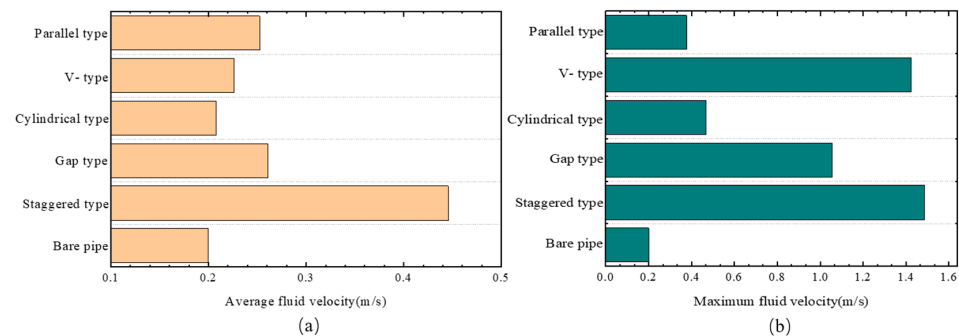


Figure 11. Variation in the (a) average fluid velocity and (b) maximum fluid velocity with different structural types.

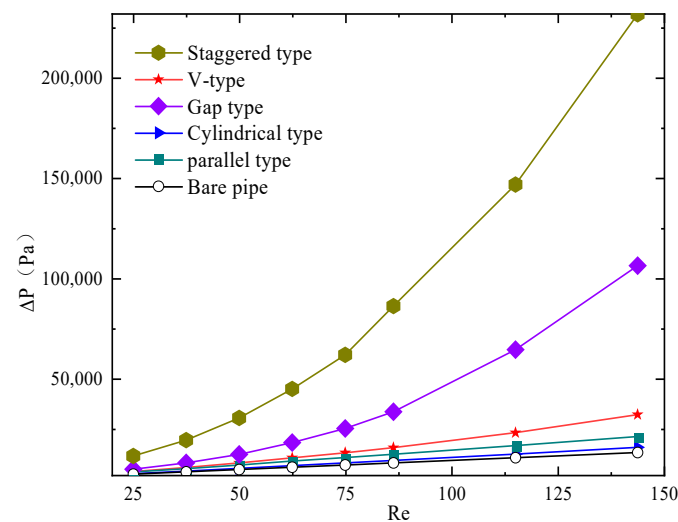


Figure 12. Variation in ΔP with Reynolds number.

Figure 13 shows the variation of the friction factor with the Reynolds number for the different enhancement structures. The friction factor decreased with an increase in the Reynolds number. The friction factor of the enhancement structures was nearly 3–5 times higher than that of the bare pipe, mainly due to the influence of the increased disturbing element on liquid flow. The greater the flow velocity at the location of the disturbing element, the stronger the obstruction effect on the fluid was. The friction factor of the cylindrical structure was almost similar to that of the bare pipe. The V and parallel types exhibited similar change trends, but the V type had a slightly higher friction factor. With an increase in the Reynolds number, the friction factors of the different enhancement structures gradually stabilized.

The variation curves of the Nusselt number with the Reynolds number for the five enhancement pipes and the bare pipe are given in Figure 14a. The heat transfer capacity of the enhancement pipe added to the perturbation element was considerably improved, and the Nusselt number of the staggered type was 180 higher than that of the bare pipe, which had a Reynolds number of 50. The Nu values of the enhancement structures increased as the Reynolds number increased, and the increase was especially pronounced at a Reynolds number of 25–75. The comparison of the data for the different enhancement structures indicated that the Nu values of the cylindrical and parallel types were close to each other. When the Reynolds number was less than 625, the Nu value of the gap type was slightly higher than that of the V type, but with an increase in the Reynolds number, the cooling

medium in the triangular area of the V type was violently disturbed, resulting in the reflux of the cooling medium and hindering the heat exchange. Although the gap type also increased the disturbance of the cooling medium when the Reynolds number was larger, the disturbance was not as severe as that of the V type, and the reflux of working fluid was relatively low due to the existence of the intermediate baffle, so the heat exchange effect of the gap type was better when the Reynolds number was greater than 625. The staggered type had the highest Nu value, which behaved particularly well. Compared with the heat transfer coefficient of the bare type (Figure 14b), the heat transfer coefficient of the staggered-type enhancement structure was higher at a Reynolds number of 114.5, followed by that of the gap- and V-type enhancement structures. The parallel-type enhancement structure had the weakest performance.

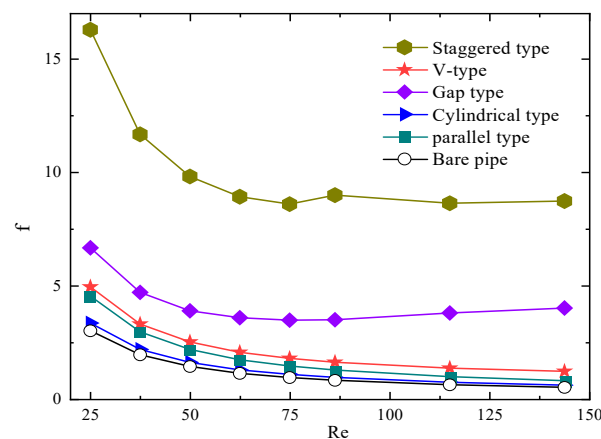


Figure 13. Variation in f with Reynolds number.

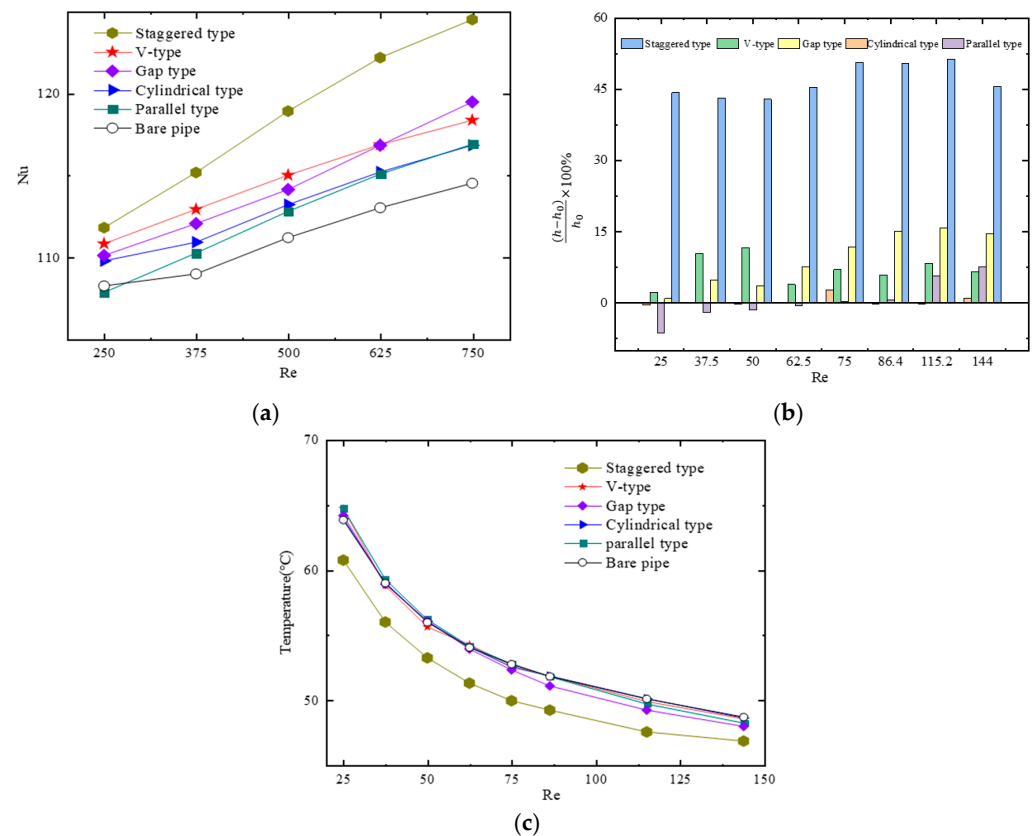


Figure 14. Variation in the (a) Nusselt number, (b) heat transfer coefficient, and (c) average wall temperature with Reynolds number.

Figure 14c shows the changes in the average wall surface temperature with the Reynolds number in pipes with different enhancement structures. The average wall surface temperature decreased with an increase in the Reynolds number, and the trends of the wall surface temperatures of the different enhancement structures were the same. The variation of the average wall surface temperature was large at a small Reynolds number. The wall surface temperature of the bare pipe had the highest average temperature, and when the staggered flat was used as the enhancement structure, the wall surface average temperature was the lowest, showing a reduction of about 3.08 °C relative to the bare pipe, followed by the gap type. Therefore, the heat transfer performance of the staggered- and gap-type enhancement structures was superior to that of the other heat transfer structures.

3.3. Comprehensive Performance Analysis

The pressure drop, convective heat transfer coefficient, Nusselt number, friction factor, and PEC corresponding to the five different enhancement structures at different flow velocities are discussed. The results indicated that the pressure drop generated by the fluid flow in the enhancement structure was larger than that in the bare pipe and that the pressure drop increased, especially when the flow velocity was high, in which case the pressure drop of the staggered enhancement structure was the largest. After the addition of an enhancement structure, the temperature of the inner wall of the whole pipe was reduced, and the maximum temperature of the pipe decreased considerably relative to that of the bare pipe. The temperature of the inner wall of the staggered structure and the pipe temperature of the gap-type structure increased with an increase in the flow velocity. At a flow velocity of 0.17 m/s, the Nusselt number in the bare pipe was 408.2, the Nusselt value in the staggered enhancement structure was 583.2, and the Nusselt value of the staggered enhancement structure was 1.43 times that of the bare pipe. The Nusselt value of the V-type structure was 1.12 times that of the bare pipe. These results show that the heat transfer performance of the enhancement structure was considerably improved compared with that of the bare pipe.

At a flow velocity of 0.5 m/s, the Nusselt number in the staggered enhancement structure was 885, which was 1.45 times that in the bare pipe. The Nusselt number of the V-type structure was only 1.05 times that of the bare pipe. As observed from the PEC value, the addition of an enhancement structure exerted a direct impact on the PEC value of the comprehensive performance index. When the inlet flow velocity was the same, the more turbulent the elements were at the same pipe length, the more obvious the effect on the fluid disturbance was, and the better the enhanced heat transfer effect was. However, if the number of spoiler elements in the enhancement structure was too large, the friction factor increased accordingly. For example, in the gap-type structure, the heat transfer effect produced by turbulence was not obvious, so increasing the number of spoiler elements had little effect. However, when the friction factor increased, its PEC value became too small. At 0.17 m/s, the friction factor of the staggered enhancement structure was about seven times that of the bare pipe, and its PEC value was 0.75. The staggered type had the highest heat exchange efficiency, but its flow resistance increased greatly. The PEC value of the cylindrical enhancement structure was close to that of the bare pipe, but the heat exchange capacity was only 70% of the capacity of the staggered type.

4. Analysis of the Optimal Enhancement Structure

4.1. Further Optimization of the Three Enhancement Structures

According to the results of screening of the enhancement structures, three types of structures, namely the staggered, gap, and V types, were further numerically studied to find the optimum structure. The simulation works were conducted with a channel pressure drop limit of 30 kPa, which is a typical value in industrial applications. Under the conditions of flow velocities of 0.19 and 0.5 m/s, structural optimization was performed by changing the number of enhancement units in the pipe. A numerical analysis was conducted on the flow and heat transfer characteristics, and the specific structure is shown in Figure 15. The

pressure drops of the three enhancement structures before and after optimization at an inlet velocity of 0.5 m/s are shown in Table 5.

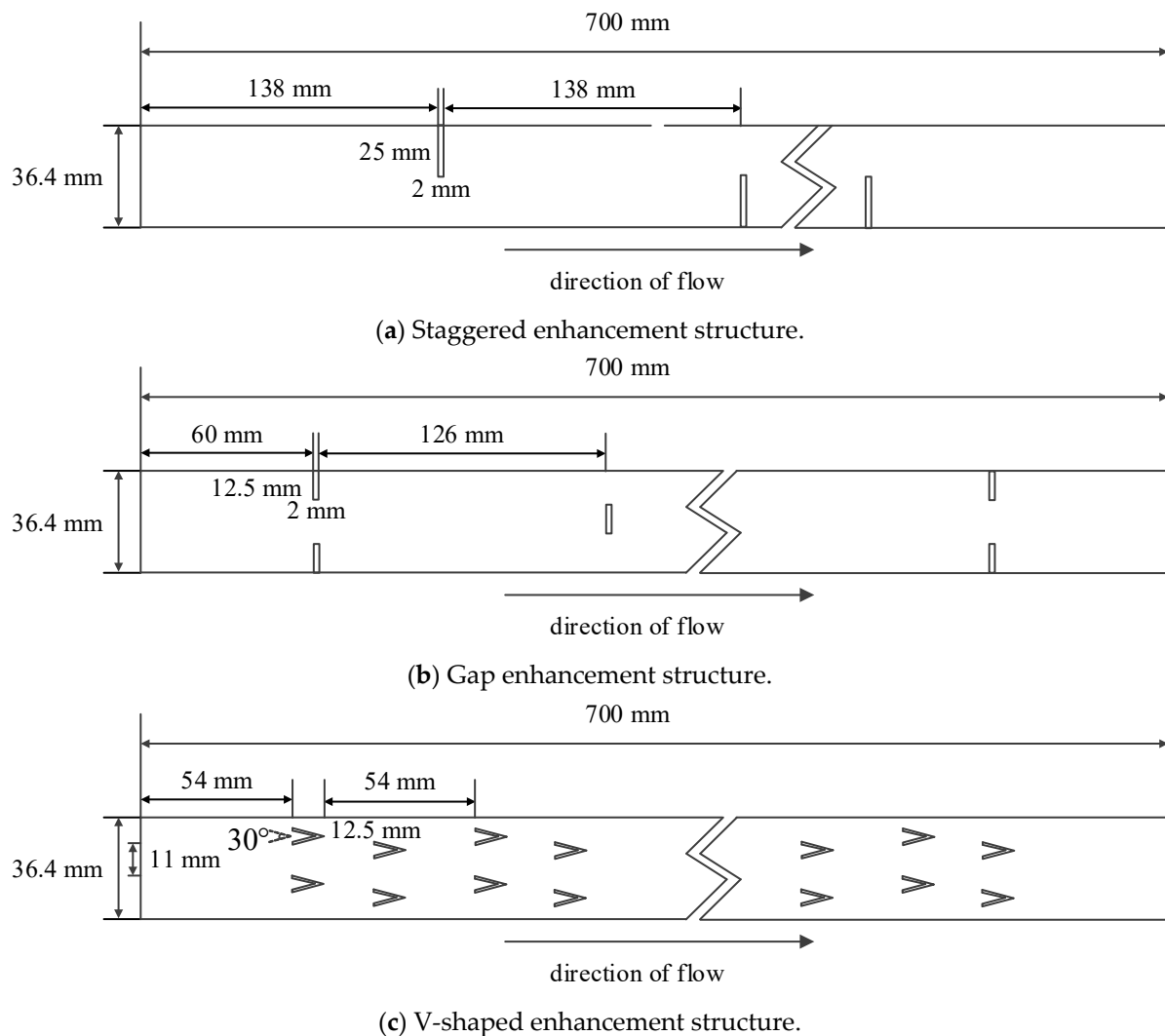


Figure 15. Arrangement of internal enhancement units in the different enhancement structures.

Table 5. Pressure drops before and after the optimization of different enhancement units.

Strengthening Structure	Optimization Status	Number of Units	Inlet Velocity (m/s)	ΔP (kPa)
Staggered type	Before optimization	40	0.5	231,811
	After optimization	8		27,372
Gap type	Before optimization	60		106,211
	After optimization	15		28,799
V type	Before optimization	54		31,816
	After optimization	42		27,495

4.2. Performance Analysis of Optimal Structures

Figure 16 shows the variation of the friction factor, pressure drop, Nusselt number, average wall temperature, and PEC of the three optimal structures at the two velocities. It indicates that increasing the flow velocity of the cooling oil can effectively improve the convective heat transfer in the pipe. The larger the Nusselt number was, the better the heat transfer performance was. The heat transfer effects of the three optimal structures at the velocity of 0.5 m/s were much higher than those at 0.19 m/s. Overall, the Nusselt number

of the gap-type structure was better than that of the V and staggered types at the same velocity, indicating that it had a more powerful heat transfer capability than the other two structures. The Nusselt number of the gap-type structure was 68% higher than that of the bare pipe. Therefore, the gap type enhanced the heat transfer in the pipe better than the other structures. The PEC value of the gap-type enhancement structure was much higher than that of the two other structures, whether at 0.19 or 0.5 m/s, which means that the gap-type enhancement structure had better heat transfer performance while performing the same pumping work compared with the other enhancement structures and bare pipes. The PEC value of the gap-type structure was improved by 39% and 63% relative to the PEC values of the staggered- and V-type enhancement structures, respectively. Thus, when the pressure drop was close to 30 kPa at the same inlet flow rate, the gap-type structure had the best heat transfer capacity and comprehensive performance. It could improve the heat transfer capacity of the pipe effectively.

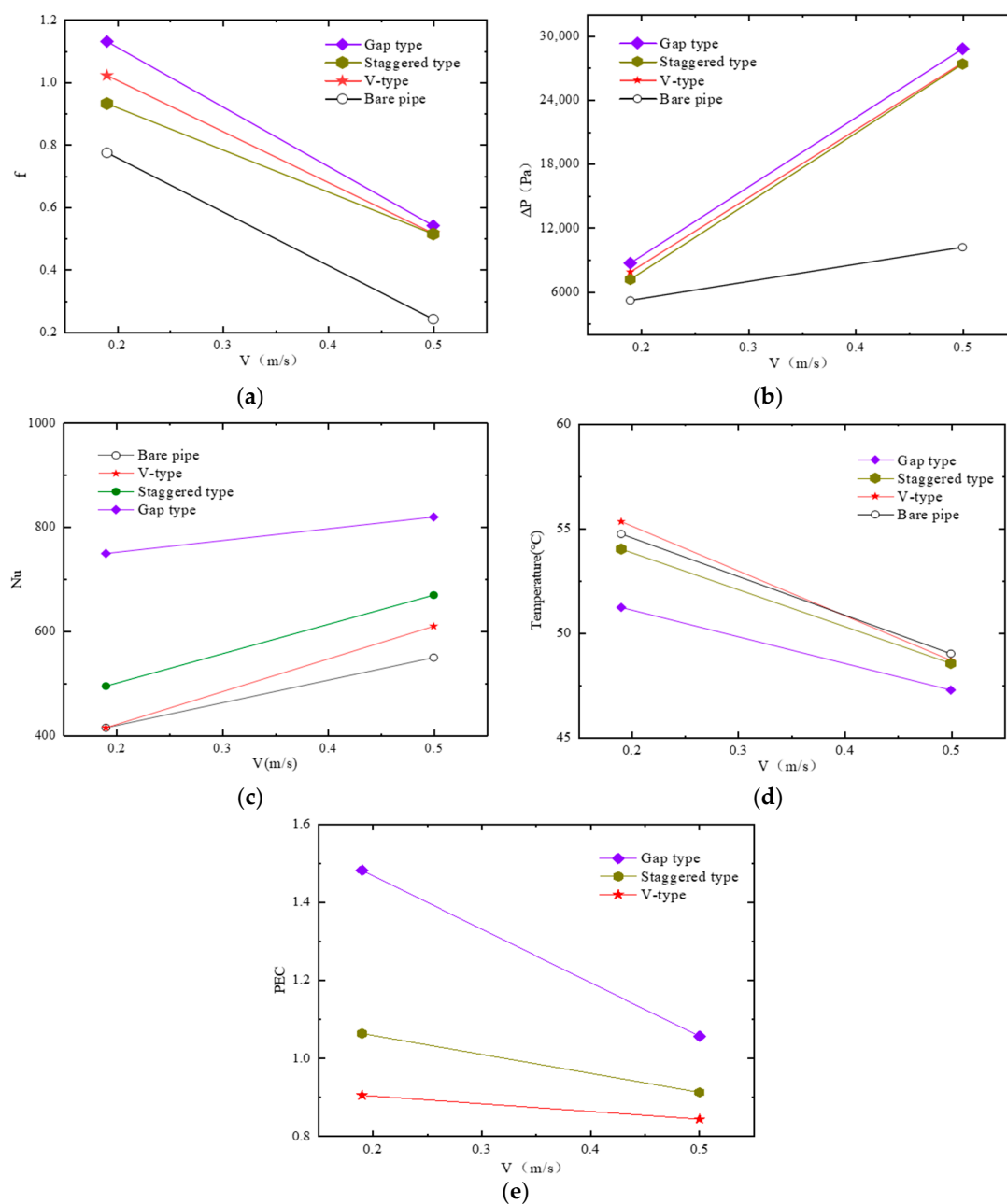


Figure 16. The (a) friction factor, (b) pressure drop, (c) Nusselt number, (d) average wall temperature, and (e) PEC of the three optimal structures at the two velocities.

Figure 17 presents a temperature distribution cloud map of the stator core, copper wire winding, and oil cooling channel. Through the performance analysis of the three enhancement structures, the temperature distribution of the key heat dissipation components of the motor was simulated to compare the temperature distribution of the oil cooling channel without the enhancement structure (Figure 17a) and the temperature distribution with optimal enhancement structure (Figure 17b) to better understand the cooling effect after adding the enhancement structure in the oil-cooling channel. When there was no enhancement structure in the oil-cooling channel, the maximum temperature of the winding was 110.28°C , the average temperature was 88.92°C , the maximum temperature of the core was 100.77°C , the average temperature was 99.08°C , and when there was an enhancement structure in the channel, the maximum temperature of the winding dropped to 98.50°C , the average temperature was 75.56°C , the maximum temperature of the core was 89.47°C , and the average temperature was 87.96°C . Compared with the motor without enhancement structure inside the oil cooling channel, the temperature of the winding and the core were significantly reduced, so the high-efficiency motor oil cooling scheme proposed in this paper, which combines the method of direct oil cooling and the optimization of the flow channel, can achieve the stable operation of the winding under high current density. This design can greatly reduce the conduction thermal resistance between the key heat source of the motor and the outside world, and the cooling effect of the motor can be maximized by optimizing the internal structure of the oil-cooling channel.

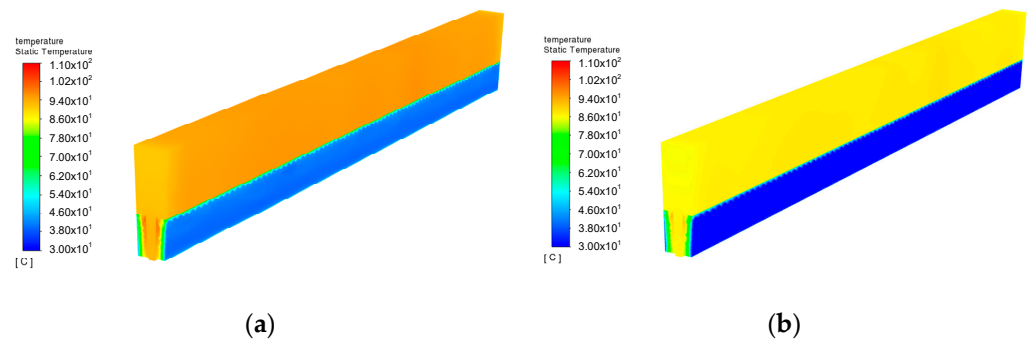


Figure 17. The (a) cooling renderings of a motor without enhancement structure, (b) cooling renderings of a motor with enhancement structure.

5. Conclusions

In this study, the influence of adding five different reinforcement structures to the oil-cooled cooling channel on the heat dissipation effect of the high-temperature superconducting armature winding was investigated by numerical simulation. The following conclusions were obtained:

- (1) The five different enhancement structures improved the heat dissipation performance of the oil cooling channel. The fluid temperature near the outlet side was higher than the outlet temperature of the bare pipe. The heat transfer performance of the gap, staggered, and V types was better than that of the cylindrical and parallel types.
- (2) The addition of the enhancement structures increased the fluid flow velocity in the pipe. The staggered structure had the highest average flow velocity, and the flow velocity changed considerably as it approached the flow velocity of the enhancement structure.
- (3) For the three types of enhancement structures with the best heat transfer performance, namely, staggered, gap, and V types, structural optimization was conducted by changing the number of enhancement units in the pipe enhancement structure under the conditions of pressure drop not exceeding 30 kPa at flow rates of 0.19 and 0.5 m/s. A comprehensive evaluation of the three structures showed that at the same flow velocity, the Nusselt number of the gap-type structure was 68% higher than that of the bare pipe. Under the same pump power consumption conditions, the PEC value

of the gap-type structure increased by 39% and 63% compared with the PEC values of the staggered and V-type enhancement structures, respectively.

In general, when inserting an oil-cooling channel with different internal enhancement structures between the air gaps of the two winding coils and both sides of the stator teeth, the temperature rise of the air gap armature and core can be more suppressed compared with the bare pipes. The cooling effect of the motor can be maximized by optimizing the internal structure of the oil cooling channel, and the results of this study provide a reference for the thermal management problem of the limited heat dissipation space of lightweight high-temperature superconducting motors.

Author Contributions: Conceptualization, S.Y. and Y.W.; methodology, J.T.; software, J.C.; validation, F.L., Y.Z. and Q.D.; formal analysis, J.T.; data curation, Y.Z.; writing—original draft preparation, S.Y.; writing—review and editing, J.Z. All authors have read and agreed to the published version of the manuscript.

Funding: This research received no external funding.

Data Availability Statement: The data are not publicly available due to [The data have been reflected in the chart of the article, so the data will not be provided in this paper].

Conflicts of Interest: The authors declare that they have no known competing financial interests or personal relationships that could have appeared to influence the work reported in this paper.

Nomenclature

λ	thermal conductivity(W/(m·K))	μ	inlet velocity (m/s)
Dh	hydraulic diameter (m)	Subscripts	
Ac	cross-sectional area (m ²)	Nu_0	Nusselt number of the bare pipe
P	wetted perimeter (m)	f_0	the friction factor of the bare pipe
h	heat transfer coefficient (W/(m ² ·K))	Abbreviation	
q_w	heat flux (W)	Nu	Nusselt number
ΔT	the average temperature difference between the wall surface and the fluid (°C)	PEC	performance evaluation criterion
ΔP	the pressure difference between the inlet and outlet (Pa)	f	friction factor
Greek			

References

1. Zhou, Y.; Dong, Q.; Zheng, J. Thermal management of air-core stator for a large-capacity HTS motor. In Proceedings of the 2015 IEEE Electric Ship Technologies Symposium (Ests), Old Town Alexandria, VA, USA, 21–24 June 2015; IEEE: New York, NY, USA, 2015; pp. 109–112.
2. Li, W.; Ching, T.W.; Chau, K.T.; Lee, C.H.T. A superconducting vernier motor for electric ship propulsion. *IEEE Trans. Appl. Supercond.* **2017**, *28*, 17478276. [\[CrossRef\]](#)
3. Torrey, D.; Parizh, M.; Bray, J.; Stautner, W.; Tapadia, N.; Xu, M.; Wu, A.; Zierer, J. Superconducting synchronous motors for electric ship propulsion. *IEEE Trans. Appl. Supercond.* **2020**, *30*, 19521682. [\[CrossRef\]](#)
4. Schreiner, F.; Liu, Y.; Zhang, Y.; Gyuraki, R.; Noe, M.; Doppelbauer, M. Development of no-insulation racetrack coils wound with 2nd generation HTS tapes for a stator system for wind generators. *IEEE Trans. Appl. Supercond.* **2020**, *30*, 19420010. [\[CrossRef\]](#)
5. Zhou, Y.; Dong, Q.; Niu, X.-J.; Xu, H.; Xiong, Q.; Su, H.; Zheng, J. A pole pair segment of oil-cooling air-core stator for a 2 MW direct-drive high temperature superconducting wind power generator. *J. Electr. Eng. Technol.* **2021**, *16*, 3145–3155. [\[CrossRef\]](#)
6. Weng, F.; Zhang, M.; Lan, T.; Wang, Y.; Yuan, W. Fully superconducting machine for electric aircraft propulsion: Study of AC loss for HTS stator. *Supercond. Sci. Technol.* **2020**, *33*, 104002. [\[CrossRef\]](#)
7. Isfahani, A.H.; Vaez-Zadeh, S. Line start permanent magnet synchronous motors: Challenges and opportunities. *Energy* **2009**, *34*, 1755–1763. [\[CrossRef\]](#)
8. Lu, S.M. A review of high-efficiency motors: Specification, policy, and technology. *Renew. Sustain. Energy Rev.* **2016**, *59*, 1–12. [\[CrossRef\]](#)
9. Han, J.; Dong, J.; Wang, Y.; Wang, C.; Ge, B.; Li, W. Coupled electromagnetic-fluid-thermal analysis for end zone with electric screen in large water-hydrogen-hydrogen cooled turbine generator under different end winding extensions. *IEEE Trans. Energy Convers.* **2021**, *36*, 2703–2713. [\[CrossRef\]](#)
10. Grabowski, M.; Urbaniec, K.; Wernik, J.; Wołosz, K.J. Numerical simulation and experimental verification of heat transfer from a finned housing of an electric motor. *Energy Convers. Manag.* **2016**, *125*, 91–96. [\[CrossRef\]](#)

11. Roffi, M.; Ferreira FJ, T.E.; De Almeida, A.T. Comparison of different cooling fan designs for electric motors. In Proceedings of the 2017 IEEE International Electric Machines and Drives Conference (IEMDC), Miami, FL, USA, 21–24 May 2017; IEEE: New York, NY, USA, 2017; pp. 1–7.
12. Gilson, G.M.; Pickering, S.J.; Hann, D.B.; Gerada, C. Piezoelectric fan cooling: A novel high reliability electric machine thermal management solution. *IEEE Trans. Ind. Electron.* **2012**, *60*, 4841–4851. [[CrossRef](#)]
13. Gai, Y.; Kimiabeigi, M.; Chong, Y.C.; Widmer, J.D.; Deng, X.; Popescu, M.; Goss, J.; Staton, D.A.; Steven, A. Cooling of automotive traction motors: Schemes, examples, and computation methods. *IEEE Trans. Ind. Electron.* **2018**, *66*, 1681–1692. [[CrossRef](#)]
14. Fan, X.; Li, D.; Qu, R.; Wang, C.; Fang, H. Water cold plates for efficient cooling: Verified on a permanent-magnet machine with concentrated winding. *IEEE Trans. Ind. Electron.* **2019**, *67*, 5325–5336. [[CrossRef](#)]
15. Polikarpova, M. *Liquid Cooling Solutions for Rotating Permanent Magnet Synchronous Machines*; Lappeenranta University of Technology: Lappeenranta, Finland, 2014.
16. Kwon, Y.K.; Baik, S.K.; Lee, E.Y.; Lee, J.D.; Kim, J.M.; Kim, Y.C.; Moon, T.S.; Park, H.J.; Kwon, W.S.; Hong, J.P.; et al. Status of HTS motor development for industrial applications at KERI & DOOSAN. *IEEE Trans. Appl. Supercond.* **2007**, *17*, 1587–1590.
17. Schiefer, M.; Doppelbauer, M. Indirect slot cooling for high-power-density machines with concentrated winding. In Proceedings of the 2015 IEEE International Electric Machines & Drives Conference (IEMDC), Coeur d’Alene, ID, USA, 10–13 May 2015; IEEE: New York, NY, USA, 2015; pp. 1820–1825.
18. Li, Y.; Fan, T.; Sun, W.; Li, Q.; Wen, X. Experimental research on the oil cooling of the end winding of the motor. In Proceedings of the 2016 IEEE Energy Conversion Congress and Exposition (ECCE), Milwaukee, WI, USA, 18–22 September 2016; IEEE: New York, NY, USA, 2016; pp. 1–4.
19. Zhou, Y.; Xu, H.; Xiong, Q.; Niu, X.-J.; Xie, R.-G. Design, performance analysis, and testing of composite components for the oil-cooling air-core stator of a high temperature superconducting motor. *IEEE Trans. Appl. Supercond.* **2021**, *31*, 21053654. [[CrossRef](#)]
20. Han, N.G.; Lee, H.L.; Kim, R.H.; Beom, T.Y.; Kim, Y.K.; Ha, T.W.; Lee, S.W.; Kim, D.K. Thermal analysis of the oil cooling motor according to the churning phenomenon. *Appl. Therm. Eng.* **2023**, *220*, 119791. [[CrossRef](#)]
21. Garud, K.S.; Hwang, S.-G.; Han, J.-W.; Lee, M.-Y. Performance characteristics of the direct spray oil cooling system for a driving motor of an electric vehicle. *Int. J. Heat Mass Transf.* **2022**, *196*, 123228. [[CrossRef](#)]
22. Park, M.H.; Kim, S.C. Development and validation of lumped parameter thermal network model on rotational oil spray cooled motor for electric vehicles. *Appl. Therm. Eng.* **2023**, *225*, 120176. [[CrossRef](#)]
23. Park, J.; An, J.; Han, K.; Choi, H.-S.; Park, I.S. Enhancement of cooling performance in traction motor of electric vehicle using direct slot cooling method. *Appl. Therm. Eng.* **2022**, *217*, 119082. [[CrossRef](#)]
24. Semidey, S.A.; Mayor, J.R. Experimentation of an electric machine technology demonstrator incorporating direct winding heat exchangers. *IEEE Trans. Ind. Electron.* **2014**, *61*, 5771–5778. [[CrossRef](#)]
25. Wang, X.; Li, B.; Gerada, D.; Huang, K.; Stone, I.; Worrall, S.; Yan, Y. A critical review on thermal management technologies for motors in electric cars. *Appl. Therm. Eng.* **2022**, *201*, 117758. [[CrossRef](#)]
26. Guo, F.; Zhang, C. Oil-cooling method of the permanent magnet synchronous motor for electric vehicle. *Energies* **2019**, *12*, 2984. [[CrossRef](#)]
27. Zhang, F.; Gerada, D.; Xu, Z.; Zhang, X.; Zhang, H.; Gerada, C.; Zhu, M.; Xia, L.; Zhang, W.; Degano, M. Improved thermal modeling and experimental validation of oil-flooded high-performance machines with slot-channel cooling. *IEEE Trans. Transp. Electrif.* **2021**, *8*, 312–324. [[CrossRef](#)]
28. Chang, J.; Fan, Y.; Wu, J.; Zhu, B. A yokeless and segmented armature axial flux machine with novel cooling system for in-wheel traction applications. *IEEE Trans. Ind. Electron.* **2020**, *68*, 4131–4140. [[CrossRef](#)]
29. Liu, W.; Dai, Y.; Zhao, J.; Wang, X. Thermal analysis and cooling structure design of axial flux permanent magnet synchronous motor for electrical vehicle. In Proceedings of the 2019 22nd International Conference on Electrical Machines and Systems (ICEMS), Harbin, China, 11–14 August 2019; IEEE: New York, NY, USA, 2019; pp. 1–6.
30. Li, F.; Ma, Q.; Xin, G.; Zhang, J.; Wang, X. Heat transfer and flow characteristics of microchannels with solid and porous ribs. *Appl. Therm. Eng.* **2020**, *178*, 115639. [[CrossRef](#)]

Disclaimer/Publisher’s Note: The statements, opinions and data contained in all publications are solely those of the individual author(s) and contributor(s) and not of MDPI and/or the editor(s). MDPI and/or the editor(s) disclaim responsibility for any injury to people or property resulting from any ideas, methods, instructions or products referred to in the content.